Electrically induced drop detachment and ejection

Andrea Cavalli, Daniel J. Preston, Evelyn Tio, David W. Martin, Nenad Miljkovic, Evelyn N. Wang, Francois Blanchette, and John W. M. Bush

Electrically induced drop detachment and ejection

Andrea Cavalli,[1] Daniel J. Preston,[2] Evelyn Tio,[2] David W. Martin,[3]
Nenad Miljkovic,[4] Evelyn N. Wang,[2] Francois Blanchette,[3]
and John W. M. Bush[5,a)]

[1]*Physics of Complex Fluids and MESA+ Institute for Nanotechnology, University of Twente,
Enschede, The Netherlands*
[2]*Department of Mechanical Engineering, Massachusetts Institute of Technology,
Cambridge, Massachusetts 02139, USA*
[3]*University of California at Merced, Merced, California 95343, USA*
[4]*Department of Mechanical Science and Engineering, University of Illinois,
Urbana, Illinois 61801, USA*
[5]*Department of Mathematics, Massachusetts Institute of Technology, Cambridge,
Massachusetts 02139, USA*

A deformed droplet may leap from a solid substrate, impelled to detach through the conversion of surface energy into kinetic energy that arises as it relaxes to a sphere. Electrowetting provides a means of preparing a droplet on a substrate for lift-off. When a voltage is applied between a water droplet and a dielectric-coated electrode, the wettability of the substrate increases in a controlled way, leading to the spreading of the droplet. Once the voltage is released, the droplet recoils, due to a sudden excess in surface energy, and droplet detachment may follow. The process of drop detachment and lift-off, prevalent in both biology and micro-engineering, has to date been considered primarily in terms of qualitative scaling arguments for idealized superhydrophobic substrates. We here consider the eletrically-induced ejection of droplets from substrates of finite wettability and analyze the process quantitatively. We compare experiments to numerical simulations and analyze how the energy conversion efficiency is affected by the applied voltage and the intrinsic contact angle of the droplet on the substrate. Our results indicate that the finite wettability of the substrate significantly affects the detachment dynamics, and so provide new rationale for the previously reported large critical radius for drop ejection from micro-textured substrates. © *2016 AIP Publishing LLC.* [http://dx.doi.org/10.1063/1.4940213]

I. INTRODUCTION

Deformed liquid drops or sheets generally store significant amounts of excess surface energy that can be efficiently converted into other forms, such as kinetic energy, when they relax to a spherical form. Surface tension dominates volume forces, such as gravity, on millimetric and sub-millimetric length scales, making it an important source of micro-mechanical actuation. In nature, several fungi of the Ballistospore family exploit related drop ejection mechanisms to release spores into the environment.[1,2] Similarly, cicadas clean their superhydrophobic wings by exploiting the recoil of coalescing microdroplets, which entrain dust and other debris when they detach from the wing surface.[3] These phenomena have sparked an interest in spontaneous drop detachment and lift-off, with several authors reporting similar observations on artificial substrates. The drop recoil-and-jump mechanism has been successfully exploited for enhanced heat exchange,[4–8] as the spontaneous jump of coalescing droplets provides an efficient way to remove liquid from a cooler surface. The same physical mechanism has been applied in single-droplet, non-coalescence based, capillary-to-inertial energy conversion by melting-initiated[9,10] and electrowetting-actuated

---

a)Author to whom correspondence should be addressed. Electronic mail: bush@math.mit.edu

28, 022101-1

drop ejection,[11–14] for uses in micro-fabrication, droplet transfer across surfaces, and controlled dewetting of superhydrophobic surfaces.[15] However, these studies are primarily experimental, and the field is lacking a detailed physical model capable of predicting jumping behavior. These myriad applications motivate our study, which is aimed at better understanding the detachment dynamics, in particular the efficiency of the conversion from surface to kinetic energy. The process is, however, difficult to analyze quantitatively for several reasons. Coalescing droplets on a superhydrophobic substrate, for example, may be affected by their droplet-droplet interactions, as well as inhomogeneities on the substrate. Through studies on zero-adhesion superhydrophobic surfaces, Enright and colleagues[16,17] have underscored the importance of internal fluid dynamics on the surface-to-kinetic energy conversion mechanism. Liu and colleagues have taken a significant step towards a systematic analysis of droplet recoil and leap by studying head-on collision of microdroplets on Leidenfrost surfaces.[18,19]

In this study, we use electrowetting to induce the controlled deformation and subsequent ejection of water droplets on a solid substrate immersed in silicone oil. By applying a voltage between the conductive droplet and substrate, we significantly reduce the contact angle of the system,[20] causing the droplet to spread. We then suddenly release the voltage and observe the droplet recoiling and, under certain conditions, detaching from the substrate. We compare our observations to numerical simulations of axisymmetrically deformed droplets on substrates of finite wettability. We are, therefore, able to quantify the effect of the applied voltage in the energy balance of the jump, as well as the role of finite wettability on the threshold radius for detachment. This characterization will inform the optimization of the jumping process for a variety of engineering and technological applications.

The paper is structured as follows. In Section II, we describe the physical picture of interest, and in Section III we detail the experimental and numerical methodology used to approach it. In Section IV, we present our results, including a direct comparison between our experiments and simulations. Encouraged by the close match between the two, we proceed by exploring a broader parameter regime numerically, giving particular attention to the system's energetics. We summarize our results and suggest future directions in Section V.

II. PHYSICAL PICTURE

The physics behind electrically induced drop ejection is illustrated in Figure 1. Consider a water droplet placed on a horizontal substrate in an oil bath. We denote by γ_{ow}, γ_{sw}, and γ_{so} the oil-water, substrate-water, and substrate-oil interfacial tensions, respectively. The system is initially at equilibrium (Figure 1-I), so the small droplet[29] forms a spherical cap whose form is prescribed by the Young contact angle θ_Y of the system, defined as $\cos\theta_Y = \frac{\gamma_{so}-\gamma_{sw}}{\gamma_{ow}}$. The free energy of this configuration is

$$E_I(\theta_Y) = \gamma_{ow}\left[2\pi R(\theta_Y)^2(1-\cos\theta_Y) - \cos\theta_Y\pi R(\theta_Y)^2\sin^2\theta_Y\right]. \tag{1}$$
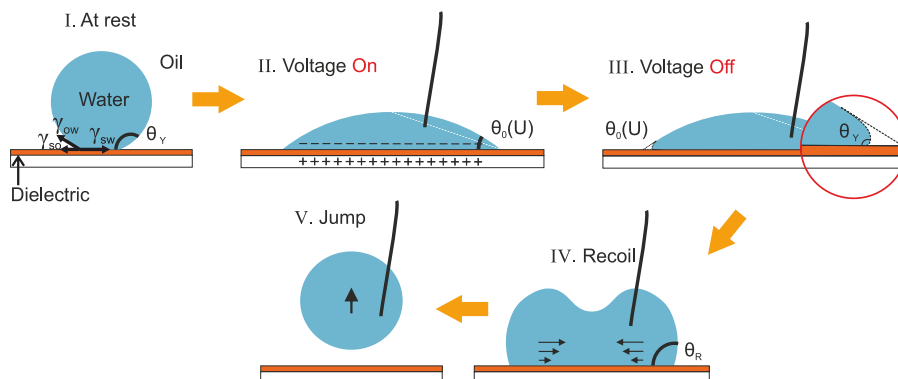

FIG. 1. A schematic illustration of the stages in electrically induced drop detachment. A water droplet is suspended in oil, then placed on a solid substrate comprising an electrode (white) and an insulating surface layer (orange).

The first term in Eq. (1) is associated with the water-oil interface, and the second with the underside of the drop. The radius of the cap is prescribed by volume conservation to be $R(\theta_Y; V) = \sqrt[3]{\frac{3V}{\pi(2-3\cos\theta_Y+\cos^3\theta_Y)}}$, where V is the drop volume. When a voltage U is applied between the droplet and an electrode below the substrate, the conducting droplet spreads on the dielectric layer, as the free charges in the water approach the counter-charges at the electrode (Figure 1-II). This process results in a reduced water-substrate surface tension γ_{sw}, and a voltage-dependent contact angle $\theta_0(U)$ described by the Young-Lippmann equation,

$$\cos\theta_0(U) = \cos\theta_Y + \frac{\epsilon_0\epsilon U^2}{2d\gamma_{ow}}, \tag{2}$$

where ϵ, ϵ_0, and d are the relative permittivity, dielectric permittivity in vacuum, and thickness of the insulating layer, respectively. The associated energy of the deformed droplet will then be

$$E_{II}(\theta_0) = \gamma_{ow}\left[2\pi R(\theta_0)^2(1-\cos\theta_0) - \cos\theta_0\pi R(\theta_0)^2\sin^2\theta_0\right]. \tag{3}$$

When the voltage is switched off (Figure 1-III), the liquid-solid surface tension suddenly increases, as the discharge of the droplet-electrode capacitor happens on a time scale much faster than the relaxation time of the droplet.[30] Consequently, the shape of the spherical cap is still as that prescribed by θ_0, but the contribution to the surface energy coming from the base of the cap now scales with θ_Y. This results in an energy

$$E_{III}(\theta_Y, \theta_0) = \gamma_{ow}\left[2\pi R(\theta_0)^2(1-\cos\theta_0) - \cos\theta_Y\pi R(\theta_0)^2\sin^2\theta_0\right]. \tag{4}$$

Since $E_{III}(\theta_Y, \theta_0)$ is always larger than the equilibrium value $E_I(\theta_Y)$, the droplet will recoil towards configuration I. This dynamic stage (Figure 1-IV) plays a key role in the efficiency of the process, as a significant fraction of the stored surface energy may be lost to the excitation of surface waves and flow-induced dissipation. However, even if the surface-to-kinetic energy conversion was perfectly efficient, the droplet would only jump if $E_{III}(\theta_Y, \theta_0)$ is larger than the minimum surface energy for a detached droplet

$$E_V = \gamma_{ow}\, 4\pi R^2(\theta_Y = \pi; V). \tag{5}$$

It is worth noting that E_V is typically larger than E_I. While a sphere represents the minimum surface energy configuration for a free droplet, here the droplet is initially (I) on the substrate, in a "bound" state whose energy is lower than that of a floating droplet. Consequently, detaching takes the droplet into an "excited" state, even in the absence of oscillations. We can thus identify $E_V - E_I$ as the work required to overcome the adhesion to the substrate. Only for extremely superhydrophobic substrates ($\theta_Y \to \pi$) does configuration V coincide with the energy minimum on the substrate, which results in zero adhesion.

Figure 2 summarizes the system energetics. Here, we plot the energy difference between stage III and V, normalized by the surface energy of a spherical droplet of the same volume (E_V). Not surprisingly, a large deformation $\theta_Y - \theta_0$ and intrinsic contact angle θ_Y both increase the energy available for the drop's jump. However, at smaller values of θ_Y, a gap opens for which $E_{III} - E_V$ is negative, and the droplet will not detach. It is worth noting that this energy ratio does not depend on the droplet volume; however, the droplet size will become relevant when the combined influence of gravity and viscous effects is considered. The dots in Fig. 2 represent the experimentally observed successful (green) or unsuccessful (red) droplet ejection. The discrepancy between this analytic model and the experimental observation can be partially explained by accounting for viscous dissipation, as we will discuss later. Another source of discrepancy is contact angle hysteresis, which would explain why the deviation is more pronounced for the Parylene-C ($\theta_Y = 130°$) substrate.

III. METHODOLOGY

A. Experiment setup

The experimental setup, shown in Figure 3, is similar to that described by Hong and Lee[12] and consists of a water droplet in a silicone oil bath placed on a conducting substrate coated
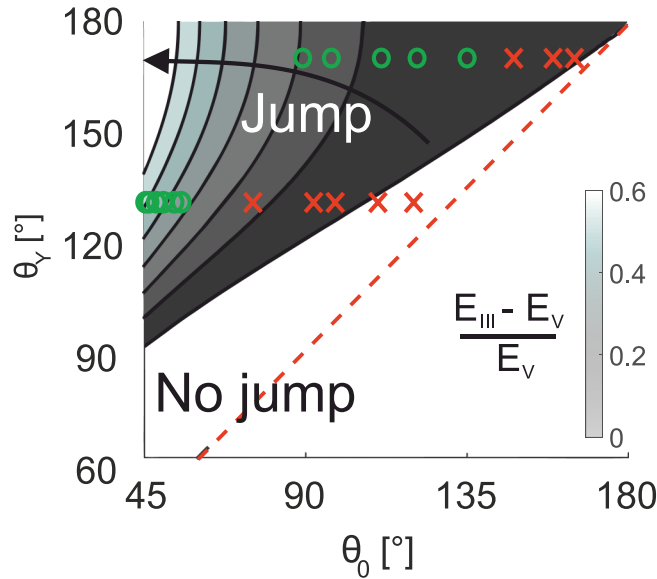
FIG. 2. Stored surface energy for a deformed droplet, as a function of the intrinsic contact angle θ_Y and the electrowetted contact angle θ_0. Dots indicate experimental results. Green circles indicate a successful jump, red crosses indicate that the droplet did not leave the substrate. The data for $\theta_Y = 170°$ are for a Teflon-coated substrate, the ones for $\theta_Y = 130°$ for a Parylene-C substrate.

with a thin dielectric layer. The substrates used in the present work are glass slides covered in a 120-160 μm thick film of indium tin oxide (ITO). The ITO films are then covered with a 4 ± 1 μm thick Parylene-C coating (VSI Parylene). The Young contact angle for these surfaces was measured to be approximately 130°. Several of the substrates were additionally dip-coated in Teflon AF to enhance hydrophobicity, resulting in a Young contact angle of 170°. Both types of substrates were employed in our experiments in order to assess the effect of the intrinsic contact angle in the detachment process. The silicone oil used for experimentation has a viscosity of 0.65 cSt and a density of 760 kg/m^3. The oil-water surface tension is approximately $\gamma_{ow} \simeq 24$ mN/m.[21] The voltage was applied to the droplet with a function generator (AFG3101, Tektronix) passed through a 100× voltage amplifier (A800, FLC electronics). A stainless steel wire with a diameter of 125 μm, inserted into the droplet, was used as the negative electrode. The experimental stage that holds the silicone oil bath was back-lit for high-speed video capture (Phantom v7.1, Vision Research) at 100 frames per second. ImageJ and Matlab were used to obtain diagnostic parameters from the high-speed video such as the base radius and height of the deformed droplet.
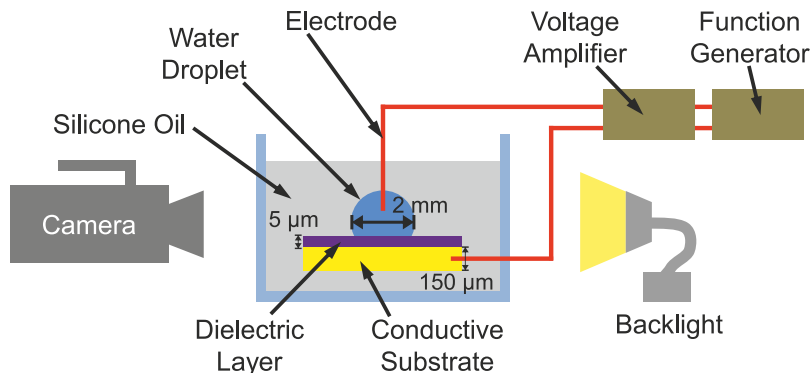

FIG. 3. Schematic of the setup employed for the electrically induced jump experiment. The conductive substrate, of thickness 150 μm, is coated with a dielectric layer of thickness 4 μm. The typical droplet volume is 5 μl.

B. Numerical simulations

In our numerical model, we consider an axially symmetric system, with a water droplet of density ρ_w and viscosity μ_w surrounded by an oil phase (with density ρ_{oil} and viscosity μ_{oil}). The equations introduced in the following are non-dimensionalized on the basis of a characteristic length scale $R_0 = \left(\frac{3V}{4\pi}\right)^{\frac{1}{3}}$, corresponding to the undeformed radius of the droplet (~ 1 mm), and a capillary time scale $T_c = \sqrt{\frac{R_0^3 \rho_w}{\gamma_{ow}}} \simeq 7$ ms. Assuming both fluids are incompressible, their evolution is governed by the Navier-Stokes equations,

$$\nabla \cdot \mathbf{u} = 0, \tag{6}$$

$$\frac{\partial \mathbf{u}}{\partial t} + \mathbf{u} \cdot \nabla \mathbf{u} = \frac{1}{\rho}\left(-\nabla p + \text{Oh} \nabla \cdot \left(\mu \left[\nabla \mathbf{u} + \nabla \mathbf{u}^T\right]\right) - c\text{Bo}\mathbf{k} + \delta_S \kappa \mathbf{n}\right). \tag{7}$$

Here, $\mathbf{u}$ is the velocity field, p the pressure, $\mathbf{k}$ is a vertical unit vector, $\mathbf{n}$ the outward unit normal to the drop surface, δ_s the two dimensional δ-function, and κ the liquid-vapor interfacial curvature. $c(\mathbf{x})$ is a marker field describing the presence of the liquid phase at a given position in the domain, ranging from 0 (oil phase) to 1 (water phase). The left hand side of Eq. (7) represents inertial forces, while the right hand side represents forces due, in turn, to pressure, viscosity, gravity, and surface tension.

The Ohnesorge and Bond numbers are defined, respectively, as

$$\text{Oh} = \frac{\mu_w}{\sqrt{R_0 \rho_w \gamma_{ow}}} \simeq \frac{\text{Viscosity}}{\sqrt{\text{Inertia} \cdot \text{Surface Forces}}}, \tag{8}$$

$$\text{Bo} = \frac{R_0^2 g \left(\rho_w - \rho_{oil}\right)}{\gamma_{ow}} \simeq \frac{\text{Gravity}}{\text{Surface Forces}}. \tag{9}$$

The Ohnesorge number prescribes the relative importance of viscosity and surface tension, the Bond number that of gravity and surface tension. The oil-water interface is tracked by Lagrangian particles that are advected by the flow. A cubic spline interpolation across the position of these trackers allows for reconstruction of the interface at each time step, as well as its intersection with the computational grid. No-slip boundary conditions for the velocity field are enforced at the floor and the ceiling of the simulation box, the exception being a local relaxation of the no-slip condition at the contact line. The drop is initialized in the electrowetted state, displaying an initial contact angle θ_0. Once the voltage is released, the droplets recoil with a fixed contact angle θ_Y. Details of the numerical implementation, as well as its convergence validation, can be found in the Appendix.

IV. RESULTS AND DISCUSSION

We begin by comparing two typical jumps from our experiments to numerical simulations with the same physical parameters. The first experiment is carried out for a water droplet of volume $\simeq 5.3$ μl. A voltage of 350 V is applied between the droplet and the Teflon-coated substrate, resulting in a reduction of the contact angle from $\theta_Y = 170°$ to $\theta_0 = 90°$. The second experiment is carried out on the Parylene-C substrate ($\theta_Y = 130°$), for a water droplet of volume $\simeq 5.5$ μl. The initial contact angle in this case is $\theta_0 = 50°$. In Figure 4 (Multimedia view), we show selected snapshots from the experiments and numerical simulations, side by side. The numerical simulation also shows the velocity magnitude $|\mathbf{u}| = \sqrt{u^2 + v^2}$, which informs the kinematics of the process.

Several dynamical features arise in both sequences. When the voltage is released, the droplet rebounds towards its intrinsic spherical cap shape. The deformation originates at the contact line, where, in less than a millisecond, the slope becomes that prescribed by θ_Y. The whole water-oil interface subsequently deforms, with mass conservation and the presence of the wall converting the initially radial motion into vertical motion[18] (between 5 and 10 ms); consequently, the drop's center of mass moves away from the substrate. At this stage, we can appreciate one of the main effects of finite wettability in this process, namely, the finite adhesion to the surface. In most experiments on superhydrophobic or Leidenfrost surfaces, the substrate acts mainly as a way to break the symmetry
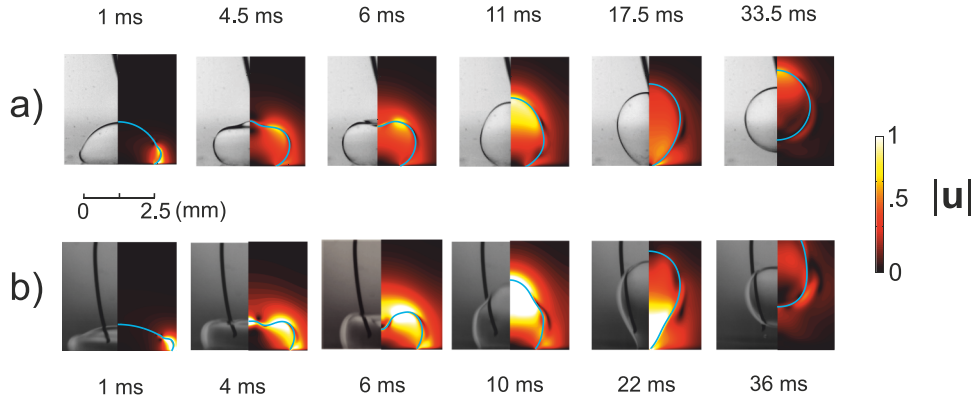
FIG. 4. (a) Selected frames showing the electrowetting-induced jump of a 5.3 μl water droplet on a Teflon AF coated substrate. (b) Selected frames for a 5.5 μl droplet on a Parylene-C coated substrate. Each frame consists of images extracted from experiments (left) and the corresponding numerical simulations (right). The velocity magnitude $|\mathbf{u}| = \sqrt{u^2 + v^2}$ in the simulations is plotted in the background in units of $v_{cap} = \frac{R_0}{T_C}$. (The movies from these experiments are available in the multimedia view.) [URL: http://dx.doi.org/10.1063/1.4940213.1] [URL: http://dx.doi.org/10.1063/1.4940213.2]

of the droplet oscillation, thus generating vertical momentum. However, since the contact angle on our substrate is finite, a fraction of the initial excess energy is spent in reducing the contact area with the substrate, rather than being purely converted into kinetic energy. The resulting development of a neck is particularly clear in Figure 4(b) (Multimedia view), where we see that the motion is initiated at the contact line, then focused towards the upward moving apex of the drop, then globally decreased as the neck develops and breaks. At this later stage, the experiment and simulation show some discrepancy: the neck snaps earlier in the numerical case, for both substrates. We believe that this deviation is due to both the presence of the needle in the experiments, which visibly affects the motion of the droplet once it detaches from the substrate, and to contact angle hysteresis at the receding contact line. Nevertheless, the maximum jump height is comparable in experiments and simulations. Note that the position of the needle relative to the droplet can be altered in order to minimize interference. For example, in applications requiring droplet transfer to an opposing surface, placing the needle in-plane with the surface and close to the drop base would reduce its influence on droplet motion. The overall agreement we observe between model and experiments is quite satisfactory, considering the relatively crude approximation (constant contact angle) made in modeling the receding contact line. A more refined model for the contact line dynamics would require the addition of a number of new parameters in our simulations, as would be required to consider the effects of dynamic contact angles and contact angle hysteresis.[22]
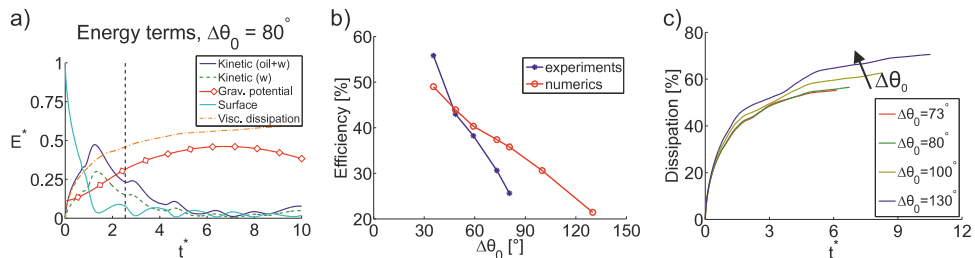

FIG. 5. (a) Energetic analysis of the jump from Figure 4(a) (Multimedia view), based on the associated numerical simulation. The black, dashed line corresponds to the detachment time. (b) The dependence of the energetic efficiency of the jump $\frac{\Delta E_G}{\Delta E_S}$ on the initial droplet deformation, from experimental data (blue line, solid markers) and numerical simulations (red line, empty markers). (c) Viscous dissipation over time, for increasing applied voltage (initial deformation) of the droplet. The time scale is normalized with the capillary time $T_c = \sqrt{R_0^3 \rho_w / \gamma_{ow}}$. The energy terms in (a) are scaled with respect to the initial excess surface energy $E_{III}(\theta_Y, \theta_0) - E_I(\theta_Y)$, as defined in Eqs. (1) and (4).

We can use the numerical simulations to extract a detailed energetic analysis of the process, which supports the qualitative observations made so far. In Figure 5(a), we report the evolution of several energy components for the simulation of Figure 4(a) (Multimedia view). All the quantities are integrated over the whole domain (oil and water phase) and scaled with respect to the initially available excess surface energy $E_{III}(\theta_Y, \theta_0) - E_I(\theta_Y)$, as defined in Eqs. (1) and (4). The transfer of excess surface energy to kinetic energy is clearly visible, with the two quantities generally varying in opposite phases. We also see that a significant amount of kinetic energy is transferred to the oil phase. The kinetic energy of the water droplet is also shown (dashed green line) for the sake of comparison. The dissipation in the system (purple line) can be quantified by integrating the rate of viscous dissipation Φ over the domain Ω, $\Phi = \int_\Omega \boldsymbol{\tau} : \nabla \mathbf{u} \, dV$, where $\boldsymbol{\tau}$ is the deviatoric stress tensor, defined as $\tau_{ij} = \mu(\partial_i u_j + \partial_j u_i)$. Note that most of the dissipation happens in the early stages of the recoil, when the droplet is flattened, so that a strong shear develops across it. After detachment (indicated by the black dashed line), the rate of viscous dissipation decreases markedly: the drop oscillations associated with the exchange between the surface and kinetic energy slowly decay.

We now discuss the efficiency of the process. Let $E_{G,0}, E_{S,0}$ be the gravitational potential and surface energy of the droplet in the initial deformed configuration, and $E_{G,h_{max}}, E_{S,h_{max}}$ the equivalent energies at the apex of the drop trajectory. The difference in surface energy, $\Delta E_S = E_{S,0} - E_{S,h_{max}}$, represents the energy available for the jump, while the increase in gravitational potential energy, $\Delta E_G = E_{G,h_{max}} - E_{G,0}$, represents the energy expended in moving the drop away from the substrate. We define the efficiency of the jump as

$$\text{Efficiency} = \frac{\Delta E_G}{\Delta E_S}. \tag{10}$$

These energy terms are both easy to extract from numerical simulations and experiment, thus allowing a direct comparison. In Figure 5(b), we plot the efficiency versus the applied voltage, for jumps from the Teflon-coated substrate. A linear correlation is indicated by both the experimental and numerical data. The higher slope for the experimental data may be partly due to the presence of the needle, which introduces another contact line in the system and so additional dissipation.

Figure 5(c) shows the viscous dissipation of energy up to the apex of the droplet trajectory, for increasing initial deformation $\Delta\theta_0$. We observe a clear similarity in the curves, which supports our previous deduction: most dissipation comes from the impulsive inward flow in the early stage of drop retraction. The energy fraction dissipated before detachment is approximately the same for all curves and is thus directly proportional to the excess surface energy stored in the initial configuration. However, a higher initial deformation results in a larger detachment speed for the droplet. Therefore, the droplet that jumps the highest also loses the most energy to viscous dissipation during the flight, which explains the decreasing efficiency of the energy conversion with $\Delta\theta_0$ reported in Figure 5(b).

Supported by the satisfactory agreement between the experiments and our numerical model, we will now employ our simulations to study the effect of the intrinsic wettability of the substrate
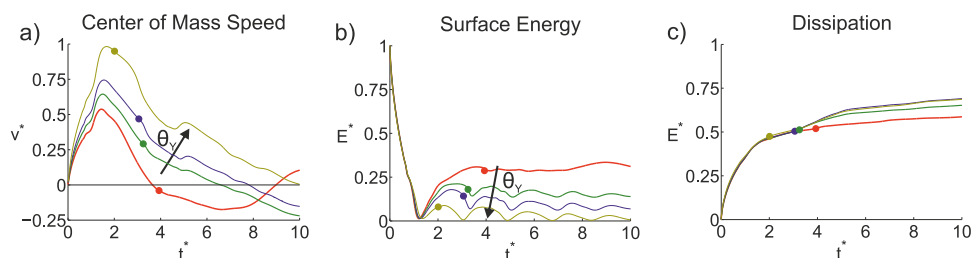

FIG. 6. Numerical simulation results indicating the evolution of the (a) center-of-mass speed, (b) surface energy, and (c) viscous dissipation, for the same initial deformation θ_0 and different θ_Y. The substrate contact angles are 110° (red), 120° (green), 130° (blue), and 170° (yellow). The time scale is normalized with the capillary time $T_c = \sqrt{R_0^3 \rho_w / \gamma_{ow}}$. The speed of the center of mass is scaled with $v_{cap} = \frac{R_0}{T_c}$. All energy terms are scaled with respect to $E_{III}(\theta_Y, \theta_0) - E_I(\theta_Y)$, as defined in Eqs. (1) and (4).

θ_Y. Several different surface treatments would be required to scan a wide range of θ_Y experimentally, for which numerical simulations provide an economical alternative. In Figure 6, we analyze simulations in which we keep the droplet volume and initial contact angle θ_0 fixed, as in the jump analyzed in Figure 4(b) (Multimedia view), while we change the substrate contact angle θ_Y. According to Eqs. (1)-(5), this should result in a higher excess energy for increasing θ_Y, as well as a lower energy barrier to jumping. In Figure 6(a), we plot the center-of-mass speed of the droplet for different values of θ_Y. We see that the average speed of the droplet in the vertical direction clearly increases with θ_Y. The maximum value is achieved when the excess surface energy (Figure 6(b)) is at a minimum: at this point, the droplet is close to its equilibrium shape. However, the droplet only takes off at the later time indicated by the dots in Figures 6(a)-6(c). By then, the speed of the droplet has significantly decreased, an effect most pronounced for small θ_Y. This can be understood by recalling Eqs. (1)-(5): before take-off, the droplet has to reduce its contact area, thus moving away from its minimum surface energy configuration. As a consequence, part of its kinetic energy is converted back to surface energy. Figure 6(b) shows the excess surface energy of the droplet with respect to a spherical cap of contact angle θ_Y. We see that the smaller θ_Y, the further the detached state is from the minimum surface energy. The wettability of the substrate thus determines not only the initially available energy but also the energy barrier to the jump resulting from adhesion to the substrate. The energy barrier to detachment thus significantly reduces the energy transferred to the center of mass motion. This effect is particularly clear for $\theta_Y = 110°$ (red, thick lines in Figures 6(a) and 6(b)), as the droplet detaches from the substrate with a negative speed in the vertical direction, and promptly falls back to the substrate. It is worth noting that this effect is completely absent in experiments on Leidenfrost substrates, where there is no contact line, so the droplet retracts unimpeded into a spherical form.

In Figure 6(c), we plot the fraction of energy dissipated over time in the oil and water phases. We see that the curves largely collapse on each other before liftoff, suggesting that the fraction of energy lost to viscosity does not depend on θ_Y, but is again proportional to the energy initially stored in the droplet, as was also evident in Figure 5(c).

Finally, we consider the interplay between wettability and droplet size in determining the smallest radius for which jumping can arise. Several authors have reported that, on superhydrophobic or Leidenfrost surfaces, the escape velocity is proportional to the capillary velocity $v_{cap} = \sqrt{\frac{\gamma_{ow}}{\rho_w R_0}}$, with a sharp viscous cutoff for small radii.[4,19] Using the non-dimensional formulation of the equations of motion, we can readily simulate droplets of different radii R using the settings of the two jumps examined in Figure 4 (Multimedia view). This is simply accomplished by rescaling the Ohnesorge number ($\propto R^{-1/2}$) and the Bond number ($\propto R^2$). As Oh increases for
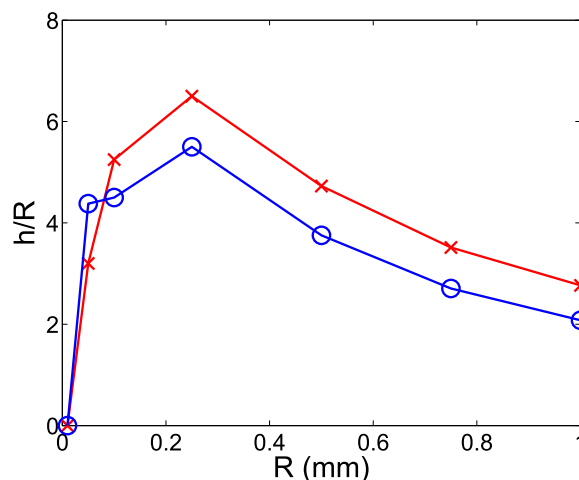

FIG. 7. Computed dependence of the normalized jump height on undeformed droplet radius $R = \left(\frac{3V}{4\pi}\right)^{\frac{1}{3}}$, corresponding to the contact angle settings of Figure 4(a) (blue, empty markers) and Figure 4(b) (red crosses).

smaller drops, we expect the dissipation to become more relevant, to the point that jumps will no longer occur for droplets smaller than a critical radius. In Figure 7, we plot the normalized jump height versus the droplet radius R. We observe that, for $R > 0.3$ mm, the normalized height slowly decreases with increasing drop size R, as the Bond number of the system increases. Conversely, for $R < 0.3$ mm, we see a sharp cutoff around 10 μm. Interestingly, Boreyko et al.[4] report a threshold radius of 10 μm for coalescing droplets on a superhydrophobic substrate, much larger than their estimation of 10 nm based on the scaling of the viscous term. While our geometry is different, we also observe a critical radius of O (10 μm) for contact angles $130° < \theta_Y < 170°$ in our simulations, suggesting that the wettability of the substrate for a large, finite contact angle could explain their discrepancy.

V. CONCLUSIONS

We have examined the detachment and jumping of droplets induced through electrical actuation. Comparing electrowetting experiments to axisymmetric numerical simulations has revealed several trends. We observe that the loss of energy to viscous dissipation is mainly localized to the early stages of the process and is roughly proportional to the excess surface energy stored in the droplet. The numerical simulations indicate that the finite wettability of the substrate does not significantly affect the energy fraction lost to viscous dissipation. However, a finite contact angle introduces an energy barrier to the droplet detachment, which reduces the height of the jump. Both these factors affect the minimum droplet radius for which detachment arises. Our simulations suggest a critical jumping radius of O (10 μm) even for large contact angles, a result consistent with previous observations of droplets coalescing on superhydrophobic surfaces.[4]

Several other parameters can be considered for further optimization of the ejection process. The timing and shape of the voltage pulse applied to the droplet will undoubtedly affect the efficiency of the energy transfer, and so the height of the jump. Another interesting topic of research would be the electric actuation of droplets on micro-textured surfaces. While the reduced adhesion to the substrate could increase the efficiency of the drop-ejection process, the electrically induced deformation might trigger a transition to a fully wetted state. An examination of this complex scenario would benefit from the combined numerical and experimental approach taken here.

In the future, it would be interesting to apply the current framework to design oil-infused surfaces,[23–25] for electrowetting-induced droplet jumping in a vapor phase environment. By infusing a superhydrophobic nanostructured surface with a low surface tension lubricant that is immiscible with the water droplet, the contact angle hysteresis can be reduced and drop detachment facilitated. Several parameters need careful consideration, such as the dielectric strength, permittivity and thickness of the oil layer, the oil-water surface energy, and the viscosity ratio of the oil and water. We note, however, that due to the low finite contact angle characteristic of water droplets on oil-infused surfaces ($\simeq 90°$–$125°$), droplet jumping in this configuration may be difficult to achieve.

ACKNOWLEDGMENTS

APPENDIX: NUMERICAL IMPLEMENTATION AND CONVERGENCE

Our numerical scheme is based on the front-tracking/finite-difference method developed by Unverdi and Tryggvason.[26,27] This method results in a sharp interface tracking, thereby avoiding the resolution issues associated with diffuse interface schemes. We solve the Navier-Stokes equations using a finite difference scheme on a staggered grid. The pressure term is handled along the lines of the projection method described by Brown.[28]

A known drawback of this approach is its inability to handle topological changes. We experimentally observe that the recoiling droplet will develop a neck, and eventually snap off from the
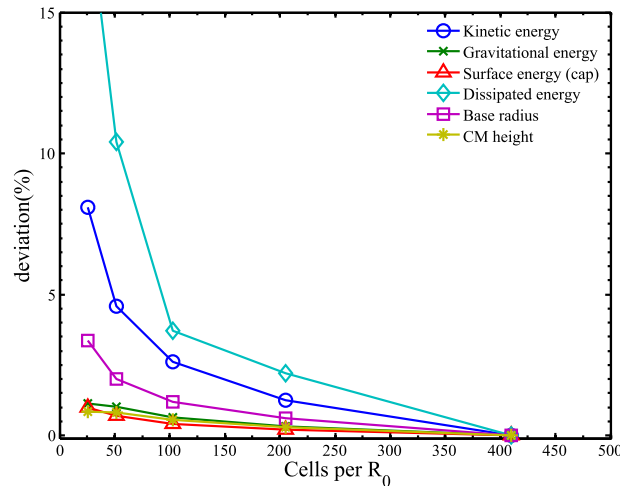
FIG. 8. Convergence analysis for a typical simulation. The percent variation of different energy terms, integrated over the domain, is plotted against the resolution of the simulation.

substrate. To reproduce this observation in the simulations, we manually disconnect the contact line once the radius of the neck reduces to $0.02R_0$ (this value corresponds to two mesh cells at our typical resolution). Another common issue with sharp interface modeling is the singularity of the stress at the contact line. To avoid this, we locally relax the no-slip boundary condition, by allowing the tracker at the solid-liquid interface to move with the velocity of the cell immediately above. This corresponds to introducing a local slip length $\lambda_S = \Delta y/2$ at the contact line, where Δy is the mesh spacing in the y-direction.[26] For the typical resolution employed, we have $\lambda_S \simeq 5$ μm. We tested the convergence of our simulations by calculating the variation of several energy terms with respect to the highest resolution simulation. The energy terms are integrated over the whole computational domain, and we average the deviation over time as $\frac{1}{n_{MAX}} \sum_{i=0}^{i=n_{MAX}} |\frac{E(t_i)-E_{h-res}(t_i)}{E_{h-res}(t_i)}|$, where $E(t_i)$ is the energy term evaluated at time step t_i, $E_{h-res}(t_i)$ is the same energy term for the highest-resolution simulation, and n_{max} is the number of time steps in the simulation. The results are shown in Figure 8, where we plot this deviation versus the linear resolution in the simulation. We can see that the deviation decreases rapidly for most energy terms, with those involving the velocity field and its derivatives showing the slowest variation. We carried out the same analysis for the height of the center of mass and the base radius of the droplet, which also show satisfactory convergence. The data in the paper were obtained using the resolution of 100 cells per $R_0 = \left(\frac{3V}{4\pi}\right)^{\frac{1}{3}}$, the characteristic radius of the droplet. A final remark concerns the energy conservation in the simulation, which we can compute by adding the conservative energy terms and the cumulative viscous dissipation inside and outside the droplet. We observe that, at the selected resolution, the energy of the system is conserved within 2%.

[1] A. Pringle, S. N. Patek, M. Fischer, J. Stolze, and N. P. Money, "The captured launch of a ballistospore," Mycologia **97**, 866–871 (2005).

[2] X. Noblin, S. Yang, and J. Dumais, "Surface tension propulsion of fungal spores," J. Exp. Biol. **212**, 2835–2843 (2009).

[3] K. M. Wisdom, J. A. Watson, X. Qu, F. Liu, G. Watson, and C.-H. Chen, "Self-cleaning of superhydrophobic surfaces by self-propelled jumping condensate," Proc. Natl. Acad. Sci. U. S. A. **110**, 7992 (2013).

[4] J. B. Boreyko and C. H. Chen, "Self-propelled dropwise condensate on superhydrophobic surfaces," Phys. Rev. Lett. **103**, 184501 (2009).

[5] J. B. Boreyko, Y. Zhao, and C.-H. Chen, "Planar jumping-drop thermal diodes," Appl. Phys. Lett. **99**, 234105 (2011).

[6] N. Miljkovic, R. Enright, Y. Nam, K. Lopez, N. Dou, J. Sack, and E. N. Wang, "Jumping-droplet-enhanced condensation on scalable superhydrophobic nanostructured surfaces," Nano Lett. **13**, 179–187 (2012).

[7] N. Miljkovic and E. N. Wang, "Condensation heat transfer on superhydrophobic surfaces," MRS Bull. **38**, 397–406 (2013).

[8] R. Enright, N. Miljkovic, J. L. Alvarado, K. Kim, and J. W. Rose, "Dropwise condensation on micro-and nanostructured surfaces," Nanoscale Microscale Thermophys. Eng. **18**, 223–250 (2014).

[9] M. Fuentes-Cabrera, B. H. Rhodes, J. D. Fowlkes, A. López-Benzanilla, H. Terrones, M. L. Simpson, and P. D. Rack, "Molecular dynamics study of the dewetting of copper on graphite and graphene: Implications for nanoscale self-assembly,"

Phys. Rev. E **83**, 041603 (2011).

[10] P. D. Rack, Y. Guan, J. D. Fowlkes, A. V. Melechko, and M. L. Simpson, "Pulsed laser dewetting of patterned thin metal films: A means of directed assembly," Appl. Phys. Lett. **92**, 223108 (2008).

[11] S. J. Lee, S. Lee, and K. H. Kang, "Droplet jumping by electrowetting and its application to the three-dimensional digital microfluidics," Appl. Phys. Lett. **100**, 081604 (2012).

[12] J. Hong and S. J. Lee, "Detaching droplets in immiscible fluids from a solid substrate with the help of electrowetting," Lab Chip **15**, 900–907 (2015).

[13] S. J. Lee, J. Hong, K. H. Kang, I. S. Kang, and S. J. Lee, "Electrowetting-induced droplet detachment from hydrophobic surfaces," Langmuir **30**, 1805–1811 (2014).

[14] J. Hong, Y. K. Kim, D.-J. Won, J. Kim, and S. J. Lee, "Three-dimensional digital microfluidic manipulation of droplets in oil medium," Sci. Rep. **5**, 10685 (2015).

[15] F. Lapierre, Y. Coffinier, R. Boukherroub, and V. Thomy, "Electro-(de) wetting on Superhydrophobic Surfaces," Langmuir **29**, 13346–13351 (2013).

[16] R. Enright, N. Miljkovic, A. Al-Obeidi, C. V. Thompson, and E. N. Wang, "Condensation on superhydrophobic surfaces: The role of local energy barriers and structure length scale," Langmuir **28**, 14424–14432 (2012).

[17] R. Enright, N. Miljkovic, J. Sprittles, K. Nolan, R. Mitchell, and E. N. Wang, "How coalescing droplets jump," ACS Nano **8**, 10352–10362 (2014).

[18] F. Liu, G. Ghigliotti, J. J. Feng, and C.-H. Chen, "Numerical simulations of self-propelled jumping upon drop coalescence on non-wetting surfaces," J. Fluid Mech. **752**, 39–65 (2014).

[19] F. Liu, G. Ghigliotti, J. J. Feng, and C.-H. Chen, "Self-propelled jumping upon drop coalescence on Leidenfrost surfaces," J. Fluid Mech. **752**, 22–38 (2014).

[20] F. Mugele and J.-C. Baret, "Electrowetting: From basics to applications," J. Phys.: Condens. Matter **17**, R705 (2005).

[21] P. Than, L. Preziosi, D. Josephl, and M. Arney, "Measurement of interfacial tension between immiscible liquids with the spinning road tensiometer," J. Colloid Interface Sci. **124**, 552–559 (1988).

[22] P.-G. De Gennes, F. Brochard-Wyart, and D. Quéré, *Capillarity and Wetting Phenomena: Drops, Bubbles, Pearls, Waves* (Springer, 2004).

[23] H. Verheijen and M. Prins, "Reversible electrowetting and trapping of charge: Model and experiments," Langmuir **15**, 6616–6620 (1999).

[24] T.-S. Wong, S. H. Kang, S. K. Tang, E. J. Smythe, B. D. Hatton, A. Grinthal, and J. Aizenberg, "Bioinspired self-repairing slippery surfaces with pressure-stable omniphobicity," Nature **477**, 443–447 (2011).

[25] A. Lafuma and D. Quéré, "Slippery pre-suffused surfaces," EPL **96**, 56001 (2011).

[26] M. Muradoglu and S. Tasoglu, "A front-tracking method for computational modeling of impact and spreading of viscous droplets on solid walls," Comput. Fluids **39**, 615–625 (2010).

[27] S. O. Unverdi and G. Tryggvason, "A front-tracking method for viscous incompressible multiphase flows," J. Comput. Phys. **100**, 25–37 (1992).

[28] D. L. Brown, R. Cortez, and M. L. Minion, "Accurate projection methods for the incompressible Navier–Stokes equations," J. Comput. Phys. **168**, 464–499 (2001).

[29] For the current analysis, the droplet is assumed to be small compared to the capillary length of the system $\lambda_c = \sqrt{\frac{\gamma_{ow}}{\Delta \rho g}}$, where $\Delta \rho$ is the density difference between the droplet and the medium oil and g is the local gravity acceleration.

[30] For a millimeter-sized water droplet on a dielectric layer of a few μm, the discharge time is $\tau \propto \frac{\epsilon}{\sigma} \sim O(\mu s)$, where σ is the conductivity and ϵ the permittivity of water. The capillary relaxation time is $T = \sqrt{\frac{R^3 \rho_w}{\gamma_{ow}}} \sim O(ms)$.[20]